



HAL
open science

Combining sclerostin neutralization with tissue engineering: an improved strategy for craniofacial bone repair

Sophie Maillard, Ludovic Sicard, Caroline Andrique, Coralie Torrens, Julie Lesieur, Brigitte Baroukh, Thibaud Coradin, Anne Poliard, Lotfi Slimani, Catherine Chaussain

► To cite this version:

Sophie Maillard, Ludovic Sicard, Caroline Andrique, Coralie Torrens, Julie Lesieur, et al.. Combining sclerostin neutralization with tissue engineering: an improved strategy for craniofacial bone repair. *Acta Biomaterialia*, 2021, 10.1016/j.actbio.2021.11.046 . hal-03466771

HAL Id: hal-03466771

<https://hal.sorbonne-universite.fr/hal-03466771>

Submitted on 6 Dec 2021

HAL is a multi-disciplinary open access archive for the deposit and dissemination of scientific research documents, whether they are published or not. The documents may come from teaching and research institutions in France or abroad, or from public or private research centers.

L'archive ouverte pluridisciplinaire **HAL**, est destinée au dépôt et à la diffusion de documents scientifiques de niveau recherche, publiés ou non, émanant des établissements d'enseignement et de recherche français ou étrangers, des laboratoires publics ou privés.

1
2
3 **Combining sclerostin neutralization with tissue engineering:**
4
5 **an improved strategy for craniofacial bone repair**
6
7
8
9

10 **Running title: Lack of sclerostin boosts bone tissue engineering**
11
12
13

14 Sophie Maillard^{1,2}, Ludovic Sicard^{1,3†}, Caroline Andrique^{1†}, Coralie Torrens¹, Julie Lesieur¹,
15 Brigitte Baroukh¹, Thibaud Coradin⁴, Anne Poliard¹, Lotfi Slimani¹, Catherine Chaussain^{1,3*}
16
17
18
19
20

21
22 ¹Université de Paris, URP2496 Pathologies, Imagerie et Biothérapies Orofaciales et Plateforme
23 Imagerie du Vivant (PIV), FHU-DDS-net, Dental School, Montrouge, France ;
24

25
26 ²AP-HP Département de parodontologie, Hôpital Rothschild, Université de Paris, France
27

28
29 ³AP-HP Services de médecine bucco-dentaire, Hôpitaux Universitaires Bretonneau, Charles
30 Foix et Henri Mondor, FHU DDS-net, Ile de France, France
31

32
33
34 ⁴Sorbonne Université, CNRS, Collège de France, Laboratoire de Chimie de la Matière
35 Condensée de Paris, 4 Place Jussieu, 75252, Paris, Cedex 05, France.
36
37
38
39
40

41 † Contributed equally to this work
42

43
44 ***Corresponding author:** Catherine Chaussain, URP2496, Université de Paris, 1 rue Maurice
45 Arnoux 92120 Montrouge, France; Tel and Fax: +33(0)158076724; email:
46 catherine.chaussain@u-paris.fr
47
48
49

50
51 **Disclosures:** none
52
53
54
55
56
57
58
59
60
61
62
63
64
65

1
2 **Abstract**
3
4
5

6 Scaffolds associated with different types of mesenchymal stromal stem cells (MSC) are
7 extensively studied for the development of novel therapies for large bone defects. Moreover,
8 monoclonal antibodies have been recently introduced for the treatment of cancer-associated
9 bone loss and other skeletal pathologies. In particular, antibodies against sclerostin, a key
10 player in bone remodeling regulation, have demonstrated a real benefit for treating osteoporosis
11 but their contribution to bone tissue-engineering remains uncharted. Here, we show that
12 combining implantation of dense collagen hydrogels hosting wild-type (WT) murine dental
13 pulp stem cells (mDPSC) with weekly systemic injections of a sclerostin antibody (Scl-Ab)
14 leads to increased bone regeneration within critical size calvarial defects performed in WT
15 mice. Furthermore, we show that bone formation is equivalent in calvarial defects in WT mice
16 implanted with *Sost* knock-out (KO) mDPSC and in *Sost* KO mice, suggesting that the
17 implantation of sclerostin-deficient MSC similarly promotes new bone formation than
18 complete sclerostin deficiency. Altogether, our data demonstrate that an antibody-based
19 therapy can potentialize tissue-engineering strategies for large craniofacial bone defects and
20 urges the need to conduct research for antibody-enabled local inhibition of sclerostin.
21
22
23
24
25
26
27
28
29
30
31
32
33
34
35
36
37
38
39
40
41
42
43
44

45 **Keywords:** Dental pulp stem cells, *Sost*/sclerostin, Tissue engineering, bone repair, dense
46 collagen hydrogel, monoclonal antibody therapy
47
48
49
50
51
52
53
54
55
56
57
58
59
60
61
62
63
64
65

1. Introduction

High bone mass diseases, namely Sclerosteosis and Van Buchem disease, are due to loss-of-function mutations of the *SOST* gene, which encodes sclerostin, a glycoprotein involved in the canonical Wnt (wingless-related integration site)/ β -catenin signaling pathway. Sclerostin, secreted primarily by osteocytes, has been shown to be a potent inhibitor of bone formation through the inhibition of the canonical Wnt signaling pathway. This pathway is activated following binding of one of the Wnt proteins and downregulated after interaction with sclerostin [1, 2] and the LRP (low-density lipoprotein receptor-related protein) 5/6 receptor [3-6]. Accumulating evidence revealed that this paracrine interaction controls cell behavior, tissue formation and bone modeling/remodeling. These observations led to extensive preclinical investigations [7-13], and to the development of several neutralizing antibodies raised against sclerostin. Their evaluation in several randomized clinical trials conducted in women with osteoporosis (romosozumab and blosozumab) [14-18], or in patients with *osteogenesis imperfecta* (setrusumab-BPS-804) [19, 20], showed that the systemic delivery of sclerostin antibodies significantly increased bone mass density through promoting osteoblast differentiation while inhibiting osteoclast formation [6, 21, 22]. Sclerostin neutralization was also shown to improve bone healing of fracture or critical-sized femoral defect in normal and pathological rodent models [23-30]. Furthermore, a tissue engineering approach based on the delivery of a miRNA targeting sclerostin was evaluated in a canine mandibular defect with positive outcomes on bone repair [31]. However, this latter approach remained isolated and no other tissue engineering strategy associated with sclerostin inhibition has been reported for bone regeneration so far.

During the last decade, mesenchymal/ stromal stem cells (MSC) have been of substantial interest to both clinicians and researchers for their considerable enhanced tissue regenerative

1 potential [32]. Indeed, their accessibility, genomic stability, high expansion *in vitro*, potential
2 for differentiation and ethical acceptability make them good stem cell candidates for tissue
3 engineering. In particular, MSC derived from the dental pulp are considered as an attractive
4 cell source for craniofacial bone regeneration due to their classical MSC properties, their easy
5 access, the less invasive approach to harvest [33-35], their identical embryologic origin [36,
6 37] and their high capacity for proliferation and differentiation into bone secreting cells [38].
7 Recent studies have shown the potential of dental pulp stem cells (DPSC) to form bone in
8 mouse models of craniofacial bone defects, indicating that DPSC were very suitable candidates
9 for the enrichment of craniofacial bone substitute [39-44]. Along this line, we previously
10 reported that murine dental pulp stem cells (mDPSC) harvested from tooth germ of *Sost* knock-
11 out (KO) mice and therefore lacking sclerostin expression exhibited a higher mineralization
12 capacity compared to their WT counterparts when exposed to mineralizing culture conditions
13 [10].

14 A large variety of biomaterials has been used as cell hosts for bone tissue engineering
15 approaches [45], including hydrogels based on natural polymers such as type I collagen [46-
16 50]. To compensate the inherent lack of structural consistence of common collagen hydrogel,
17 a “plastic compression” has been proposed to increase the relative fibrillar density [51-54],
18 resulting in a density similar to the osteoid tissue [55-58]. Supporting the interest of this
19 approach, our team has established the osteogenic potential of DPSC-seeded dense collagen
20 hydrogels implanted in rodent calvarial defects [39, 43, 44]. A strategy aiming at further
21 enhancing bone regeneration in terms of volume and quality within such constructs would
22 constitute a major therapeutic advance. In particular, recent advances in the association of
23 immunotherapy and biomaterials in the field of cancer treatment [59-61] suggest that
24 combination of such scaffolds with a neutralizing sclerostin antibody may constitute a highly
25 promising approach. Therefore, in the present study, we aimed at assessing whether the

1 neutralization of sclerostin may improve the efficacy of a tissue engineering strategy for
2 treating large craniofacial bone defects. In that purpose, we evaluated whether bone formation
3 was enhanced in parietal defects performed in wild-type (WT) mice weekly treated with a
4 systemic injection of a sclerostin antibody (Scl-Ab) during the bone regeneration process. In
5 parallel, WT mice were restored with dense collagen hydrogels enclosing *Sost* KO mDPSC
6 and compared to WT mice similarly treated with WT mDPSC. Our results show increased bone
7 formation in WT mice either under systemic pharmacological sclerostin neutralization or
8 implanted with *Sost* KO mDPSC. These observations strongly support the interest of
9 combining a tissue engineering strategy with sclerostin neutralization for the treatment of large
10 craniofacial bone defects, either through systemic injection or by local delivery.
11
12
13
14
15
16
17
18
19
20
21
22
23
24

25 **2. Materials and methods**

26 **2.1 Study design**

27
28
29 Two independent experiments have been designed in order to assess the interest of sclerostin
30 deficiency in bone regeneration. In the first experiment, a 3.5 mm critical size defect was
31 surgically created in the parietal bone in 10-week-old male *Sost* KO mice (n = 40) and wild-
32 type mice (n = 40). The defects were subject to the following conditions: (i) either left empty
33 (no collagen-hydrogel), filled, ii) with an acellular collagen-hydrogel, or with a collagen-
34 hydrogel seeded with mDPSC, iii) from WT mice (WT mDPSC) or iv) *Sost* KO mice (*Sost* KO
35 mDPSC).
36
37
38
39
40
41
42
43
44
45
46
47

48 In the second experiment, male WT mice were randomly assigned to Scl-AB (Setrusumab,
49 BPS804; kind gift from Mereo Biopharma (London, UK) (n = 10 per group) or vehicle (saline
50 solution) injection, (n = 10 per group), according to Roschger et al [62]. In brief, Scl-AB was
51 injected intravenously at a dose of 100 mg per kg body weight. Injections of Scl-AB or the
52 vehicle were given once a week over a period of eight weeks. Mice were euthanized at the end
53
54
55
56
57
58
59
60
61
62
63
64
65

1 of the eight-week intervention period, i.e., at the age of 18 weeks. Body weights were recorded
2 at the time of each injection.
3
4

5 **2.2 Ethical approval and animal management**

6 All experiments in this study were conformed to ARRIVE (Animal Research: Reporting of *in*
7 *vivo* Experiments) guidelines and were approved by the Animal Care Committee of the
8 Université de Paris (APAFIS agreement # 24297 N°2019022017023656). Animals were
9 maintained according to the guidelines for ethical conduct developed by the European
10 Communities Council Directive (animal breeding agreement C92-049-01). All efforts were
11 made to minimize their pain or discomfort. Hundred forty ten-week-old male mice (100 WT
12 and 40 *Sost* KO) with a C57BL/6J genetic background were used for this study[10] and were
13 housed in stable conditions ($22 \pm 2^\circ\text{C}$) with a 12 h dark/light cycle and with *ad libitum* access
14 to water and food.
15
16
17
18
19
20
21
22
23
24
25
26
27
28
29
30

31 **2.3 Isolation and culture of Dental Pulp Stem Cells from PN3 WT or *Sost* KO mice**

32 Multi-colony-derived mouse dental pulp stem cells were obtained from the molars of three-day
33 postnatal (PN3) littermate *Sost* KO mice and WT mice using a protocol adapted from [36][10].
34 Briefly, murine molar gems were collected under sterile conditions and incubated at 4°C for
35 45 min in phosphate-buffered saline (PBS) containing 100 U/ml penicillin/streptomycin
36 (Gibco, Hampton, USA) and 250 $\mu\text{g/ml}$ fungizone (Gibco), then in PBS containing three
37 mg/ml type I collagenase (Worthington Biochem, Freehold, NJ, USA) and two U/ml dispase I
38 (Roche, Mannheim, Germany) in a shaking incubator (at 37°C) for one hour. The isolated cells
39 were then plated on 0.1% gelatin-coated dishes in the Minimum Essential Media-alpha (Gibco)
40 supplemented with 20% v/v fetal bovine serum (FBS) (Gibco) and 100 U/ml
41 Penicillin/streptomycin (Gibco), 2.5 ng/ml FGF-2 (PeproTech, Neuilly-Sur-Seine France),
42 10 ng/ml BMP-2 (PeproTech), and maintained at 37 °C under 5% CO₂ atmosphere. The
43
44
45
46
47
48
49
50
51
52
53
54
55
56
57
58
59
60
61
62
63
64
65

1 medium was changed after two days, and then twice a week. The required cell number for *in*
2 *vivo* experiments was reached after two to three passages.
3
4

5 **2.4 Collagen-hydrogel preparation**

6 Plastically compressed collagen gels were used as three dimensional scaffolds and prepared as
7 previously described [52, 63, 64]. Briefly, 3.2 ml of sterile rat-tail collagen type I (First Link
8 Ltd., Wolverhampton, U.K.) at a protein concentration of 2.0 mg/ml in 0.1% acetic acid was
9 mixed with 0.4 ml of 10X Dulbecco's Modified Eagle Medium (DMEM) and neutralized by
10 0.4 ml 10X HCO³⁻ and drop-wise addition of 0.1 N NaOH to pH 7.4 [65]. After neutralization,
11 acellular or with mDPSC at a seeding density of 2.10⁶ cell/ml was ice-cold mixed and 0.9
12 ml/well of the mix was plated into a four-well plate. After gelling (30 min at 37 °C), highly
13 hydrated hydrogels were placed on a stack of blotting paper, nylon, and stainless steel meshes.
14 Dense collagen hydrogels were produced by the application of an unconfined compressive
15 stress of one kPa for five min to remove excess casting fluid. The compressed scaffolds were
16 circularly cut (four mm diameter) and kept up to 24 h at 37 °C under 5% CO₂ in serum-free
17 medium before implantation [66].
18
19
20
21
22
23
24
25
26
27
28
29
30
31
32
33
34
35
36
37

38 **2.5 Surgical implantation**

39 Mice were anesthetized (100 mg/kg b.w. of ketamine and 10 mg/kg b.w. of xylazine
40 hydrochloride, both from Centravet Alfort, Maisons-Alfort, France). In each specimen, scalp
41 skin was incised, and the periosteum was eliminated to visualize the skull. A 3.5 mm diameter
42 calvarial critical-sized defect was created on each side of the parietal bone using a dental bur
43 attached to a slow-speed hand piece operating at 1500 rpm, under irrigation with sterile saline
44 solution [67]. Special care was taken for the sagittal suture preservation, and minimal invasion
45 of the dura mater. After gently removing the circular bone plug, a mDPSC-seeded dense
46 collagen-hydrogel or acellular dense collagen-hydrogel prepared as previously described was
47
48
49
50
51
52
53
54
55
56
57
58
59
60
61
62
63
64
65

1 implanted in bone defect (n = 280 hydrogels for the entire experiment (n°1 and 2): acellular
2 hydrogel, hydrogel seeded with WT mDPSC or hydrogel seeded with *Sost* KO mDPSC. Each
3
4 animal was randomly allocated per cage and per group and received the same treatment on both
5
6 sides. Wound closure was achieved by a suturing (periosteum, skin) using absorbable sutures
7
8 (Vicryl Rapid 5.0 and 4.0 respectively, Ethicon, Johnson & Johnson). Immediate post-
9
10 operative care included analgesia with buprenorphine (0.02 mg/kg b.w.). After surgery, the
11
12 animals were housed individually under constant conditions. No lethality was detected during
13
14 the surgery or the post-operative period. Wound healing progressed without any sign of
15
16 infection, material exposure or other complication. Body weights were examined regularly to
17
18 ensure proper feeding before and after surgery.
19
20
21
22
23
24

25 **2.6 Micro-X-ray computed tomography (Micro-CT) examination of samples.**

26
27 For bone regeneration exploration, mice were anesthetized (isoflurane, induction at 2–2.5%
28
29 under airflow of 0.8–1.5 L/min; 1–1.5% under 400–800 ml/min thereafter) and were imaged
30
31 using an X-ray micro-CT device (Quantum FX Caliper, Life Sciences, Perkin Elmer, Waltham,
32
33 MA) hosted by the PIV Platform, URP2496, Montrouge, France. The X-ray source was set at
34
35 90 kV for the voltage and 160 μ A for the intensity. Tridimensional images were acquired with
36
37 an isotropic voxel size of 20 μ m. Full three dimensional high-resolution raw data are obtained
38
39 by rotating both the X-ray source and the flat panel detector 360° around the sample (scanning
40
41 time: 3 min). Tridimensional rendering was subsequently extracted from DICOM image stacks
42
43 using the open-source OsiriX imaging software (v5.7.1, distributed under LGPL license, Dr A.
44
45 Rosset, Geneva, Switzerland) [68]. Before quantification, image stacks were reoriented using
46
47 DataViewer (Skyscan, release 1.5.2.4, Kontich, Belgium) to the center of the defect. Then,
48
49 quantification of the regenerated bone was performed with a cylindrical shape volume of
50
51 interest of 3.5 mm of diameter and 1 mm height, using CT-Analyzer software (Skyscan, release
52
53 1.13.5.1, Kontich, Belgium). An adaptative thresholding was performed with a radius of two,
54
55
56
57
58
59
60
61
62
63
64
65

1 between 364.34 and 560.82 mgHA/cm³ (HA: Hydroxyapatite). To reduce background,
2 open/close morphological operations (radius = 1) were performed on the segmented bone.
3
4 Bone volume fraction BV/TV (BV: Bone volume and TV: Total volume) (%), porosity (mm⁻³)
5 and Bone Mineral Density (BMD, mgHA/cm³) were used to quantify and characterized
6
7 newly repaired bone. Since the regenerated bone is mainly a compact bone, trabecular
8
9 thickness Tb.Th (mm), trabecular number Tb.N (one per mm) and trabecular separation Tb.Sp
10
11 (mm) were not described due to the fact that these values are specific to trabecular bone [69].
12
13
14
15
16

17 **2.7 Histology, histomorphometry**

18 Two-months non-decalcified samples (n=6 defects per condition) were fixed in 70% vol/vol
19 ethanol (24 hours at 4°C), dehydrated in graded ethanol solutions and embedded at -20°C in
20 methacrylate resin (Merck & Co., Whitehouse Station, NY) [70]. Five-µm thick deplastified
21 calvaria bone sample sections were sequentially cleared in water and stained with von Kossa
22 staining, or processed for alkaline phosphatase (ALP) enzyme-histochemistry and for tartrate-
23 resistant acid phosphatase (TRAP) revelation [43]. Von kossa staining was used to visualize
24 mineralized bone. TRAP was detected by using hexazotized pararosanilin (Sigma) and naphthol
25 ASTR phosphate (Sigma, St Louis, MO) to reveal osteoclasts; non-osteoclastic acid
26 phosphatase was inhibited by adding 100 mMol/L L(+)-tartric acid (Sigma, St Louis, MO) to
27 the substrate solution.
28
29
30
31
32
33
34
35
36
37
38
39
40
41
42
43
44

45 **2.8 Image acquisition and quantification**

46 Image acquisition was performed using a Lamina multilabel slide scanner (Perkin Elmer)
47 hosted by the HistIM platform at the Institut Cochin, Paris. Slide visualization was performed
48 with CaseViewer, 3DHISTECH's advanced slide viewing software, and images were analyzed
49 using Fiji (*Fiji Is Just ImageJ*) [71], an open source image processing package based on ImageJ
50
51 (six sections were counted for each sample).
52
53
54
55
56
57
58
59
60
61
62
63
64
65

2.9 Second harmonic Generation (SHG) Microscopy

Second harmonic generation microscopy offers the opportunity to image and quantify collagen without staining, and was used as previously described [72]. Briefly, a multiphoton inverted stand Leica SP5 microscope (Leica Microsystems GmbH, Wetzlar, Germany) hosted in the IMAG'IC facility at the Institut Cochin, Paris, was used for calvaria imaging. A Ti:Sapphire Chameleon Ultra (Coherent, Saclay, France) with a center wavelength at 810 nm was used as the laser source for generating second harmonic (SHG) and two-photon-excited fluorescence (TPEF) signals. The laser beam was circularly polarized. A Leica Microsystems HCX IRAPO 25×/0.95 W objective was used to excite and collect SHG and TPEF signals.

Signals were detected in epi-collection through 405/15 nm and 525/50 bandpass filters, respectively, by NDD PMT detectors (Leica Microsystems) with a constant voltage supply, at constant laser excitation power, allowing the direct comparison of SHG intensity values. LAS software (Leica, Germany) was used for laser scanning control and image acquisition. Analyses were performed using a homemade ImageJ routine. Two fixed thresholds were chosen to distinguish biological material from the background signal (TPEF images) and specific collagen fibers. The SHG score was established by comparing the area occupied by the collagen relative to the sample surface.

2.10 Statistical analysis

Numerical variables are expressed as the mean \pm standard error of the mean (S.E.M). The statistical analyses were performed using Prism software version 7.04 (GraphPad software, La Jolla, CA). The normality of the distribution was tested with the D'Agostino-Pearson omnibus normality test and the homogeneity of variance was tested with the Fisher F test. Since data was following a normal distribution and variances were significantly different between groups, a Brown-Forsythe and Welch ANOVA parametric test allowing the comparison between more than two independent samples was performed. As two defects were performed for each animal,

1
2
3 it was the bone defect that was considered as the statistical unit. Differences were considered
4
5
6 significant at $P < 0.05$.

7 **3. Results**

8 9 **3.1 The implantation of *Sost* KO mDPSC in WT mice potentiates the outcomes of a** 10 11 **tissue engineering strategy**

12
13
14 To assess the interest of the inhibition of sclerostin for a tissue engineering approach, we first
15
16 investigated bone formation in calvarial defects performed in WT mice and implanted with
17
18 hydrogels enclosing *Sost* KO mDPSC, in comparison to WT mice implanted with hydrogels
19
20 enclosing WT mDPSC (Fig.1,2). The MSC nature of these cells has been previously
21
22 established [44, 73]. *Sost* KO mice, which have been shown to display a strong bone formation
23
24 potential [11, 74], were treated similarly as a positive control. For each genotype, four different
25
26 conditions were applied i) defect left empty (no hydrogel), ii) defect filled with a dense
27
28 acellular collagen hydrogel, iii) defect filled with a dense collagen hydrogel enriched with WT
29
30 mDPSC, and iv) defect filled with a dense collagen hydrogel enriched with *Sost* KO mDPSC.
31
32 Bone healing was analyzed by micro-CT at two months (Fig.1a) and further characterized by
33
34 histology. Micro-CT analyses indicated that neither WT nor *Sost* KO parietal defects left empty
35
36 experienced bone repair at the center of the defects, confirming the critical size defect nature
37
38 of our model even in *Sost* KO animals (Fig.1a). For all the other conditions, bone formation
39
40 was observed at both the edge and the center of the defects. As expected [11, 74], increased
41
42 BV/TV was systemically found in *Sost* KO mice when compared to their WT counterparts and
43
44 the addition of mDPSC, either WT or KO, did not improve bone formation in KO animals
45
46 (Fig.1a). In contrast, in WT mice, the addition of mDPSC significantly improved bone
47
48 formation compared to acellular hydrogels. Furthermore, WT mice treated with *Sost* KO
49
50 mDPSC-seeded hydrogels displayed a significantly higher BV/TV compared to WT mice that
51
52
53
54
55
56
57
58
59
60
61
62
63
64
65

1 received WT cells ($P < 0.0001$). The BV/TV measured in WT mice treated with *Sost* KO cells
2 was not significantly lower than those obtained in the positive control (*Sost* KO mice).
3

4 Both ALP, which reflects osteoblast activity, and von Kossa staining, which shows mineral
5 formation, were robust in *Sost* KO mice and in WT mice treated with *Sost* KO mDPSC (Fig.1b;
6
7 c). Quantification of Von Kossa staining confirmed these observations. Consistent with our
8
9 micro-CT findings, WT mice treated with *Sost* KO cells showed a significantly higher
10
11 percentage of mineralized tissue in the defects compared to WT mice treated with WT cells
12
13 (Fig.1b; $P < 0.001$). Of note, in *Sost* KO mice, the addition of KO cells significantly improved
14
15 mineral deposition when compared to the addition of WT cells. We then explored osteoclast
16
17 resorption activity within the defects by assessing TRAP activity (Fig. 2a). No significant
18
19 difference was found for either WT or *Sost* KO mice treated with WT or KO cells, indicating
20
21 that, in our model, *Sost* deletion favors bone formation but does not influence resorption
22
23 (Fig.2a). We next investigated the newly formed bone using second harmonic generation
24
25 (SHG) microscopy (Fig. 2b). Red-labeled well-organized bundles of collagen fibers were
26
27 observed within the defects performed in WT and *Sost* KO mice treated with either WT or KO
28
29 cells, indicating that the addition of mDPSC within the hydrogels favors matrix reorganization.
30
31 However, analysis of the bone porosity and density from micro-CT acquisitions showed no
32
33 benefit for the addition of mDPSC in the hydrogel either in WT or *Sost* KO mice, indicating
34
35 that even if more bone is formed in KO mice and in WT mice treated with KO cells, these
36
37 microarchitecture parameters are not improved at this stage of the repair process by the *Sost*
38
39 deletion (Fig. 2c).
40
41
42
43
44
45
46
47
48
49

50 Taken together, these data showed increased bone formation in WT animals implanted with
51
52 *Sost* KO mDPSC at two months. The deletion of *Sost* in the implanted cells displayed a similar
53
54 potential to stimulate bone formation than *Sost* KO animals treated with WT or KO cells.
55
56
57
58
59
60
61
62
63
64
65

3.2 Systemic Scl-Ab treatment potentiates the outcomes of tissue engineering strategy in

WT mice

Based on our data showing improved bone repair in the defects performed in WT mice treated with *Sost* KO mDPSC, we sought to investigate whether the administration of a sclerostin-neutralizing Scl-Ab [19, 20] to WT mice may improve a tissue engineering strategy (dense collagen hydrogels enriched with mDPSC). To this end, the bone repair process within calvarial defects, either empty or filled with acellular or WT mDPSC cellularized hydrogels, was analyzed after two months in WT mice weekly injected with Scl-Ab or vehicle (Fig.3,4). Representative three dimensional images of bone defects created in WT and *Sost* KO mice in four conditions (Fig.3a) revealed a complete closure of the defect in mice treated with the Scl Ab and a hydrogel enclosing mDPSC, and an almost complete one for the acellular hydrogels (Fig.3a). The quantitative analysis highlights that the BV/TV was significantly higher in the Scl Ab -treated animals compared to the vehicle injection (Fig.3a). Noteworthy, in these Scl Ab -treated animals, the addition of mDPSC in the hydrogel significantly improved bone repair when compared to acellular controls ($P < 0.0001$). Accordingly, ALP staining indicated a strong osteoblast activity in this condition (WT mDPSC combined with Scl-Ab) (Fig.3b), and Von Kossa staining revealed a significantly higher amount of mineralized tissue formation with Scl-Ab injection than in vehicle-only controls (Fig.3c). Furthermore, in these Scl Ab -treated animals, the addition of WT mDPSC further improved mineralization when compared with the “acellular hydrogel” condition ($P < 0.01$) (Fig. 3c). In contrast, no difference regarding osteoclast activity was found in this group, suggesting that the antibody rather targets bone formation than bone resorption at the stage of the process (Fig. 4a).

Next, we investigated the quality of the newly formed bone using SHG microscopy (Fig. 4b). This analysis indicated better collagen fiber organization in mice treated with the Scl-Ab when compared to the vehicle for all the conditions, but this observation was particularly striking for

1 cellularized defects. Analysis of the bone porosity and density from micro-CT acquisitions
2 showed a significantly lower porosity in defects performed in animals treated with the Scl-Ab
3 compared to vehicle (Fig.4c). However, at this stage of the bone repair process, the addition of
4 cells did not impact these microarchitecture parameters. Taken together, these data show higher
5 bone formation with upregulation of the osteoblastic activity within the calvarial defects in
6 cellularized tissue engineered constructs associated with Scl-Ab injection.
7
8
9
10
11
12
13
14
15
16

17 **4. Discussion**

18 Tissue engineering appears as a promising option to treat large bone defects [45], especially in
19 the context of the craniofacial area, which requires extremely difficult surgical reconstructions.
20 Here, we have raised the hypothesis that a tissue engineering strategy, namely implantation of
21 dense collagen hydrogels enclosing mDPSC, combined with the inhibition of sclerostin may
22 greatly enhance bone regeneration within critical size calvarial defects. Our data show that
23 sclerostin neutralization by the systemic injection of a sclerostin antibody [19, 20], a strategy
24 already used to treat osteoporosis and other bone diseases [6, 21, 75, 76], markedly improves
25 the outcomes of our tissue engineering approach, resulting in higher bone formation in animals
26 treated with both Scl-Ab and hydrogels, and especially with those enriched with mDPSC.
27
28
29
30
31
32
33
34
35
36
37
38
39
40

41 The use of the dental pulp as source of MSC appears fully justified here as most of the
42 craniofacial bones and the dental pulp MSC share a common neural crest embryological origin
43 [37, 77]. In addition, neural-crest derived osteogenic cells are known to be more efficient in
44 osteoblast differentiation and bone repair than their mesoderm counterparts [78]. Regarding
45 the use of dense collagen hydrogels as a scaffold, we and others have previously demonstrated
46 that such scaffolds allowed the addition of MSC and a fiber density favoring osteogenesis,
47 while being perfectly tolerated by the host upon implantation [39, 44, 52, 55, 56, 58, 79]. In
48 our study, the addition of DPSC within the dense collagen hydrogels markedly improved bone
49
50
51
52
53
54
55
56
57
58
59
60
61
62
63
64
65

1 regeneration in WT mice, which is consistent with previous studies in rodent models [39, 43,
2 44, 56, 73]. This observation is true for our two sets of experiments despite the fact that the
3 amount of newly formed bone differed between these experiments. This may be due to the fact
4 that these experiments were conducted independently, at different time of the year and with
5 different batches of cells and reagents.
6
7
8
9
10

11 The benefit of mDPSC addition was less marked in *Sost* KO mice, as bone formation was
12 comparable in acellular hydrogels and hydrogels enriched with mDPSC harvested from WT or
13 KO molar germs (Fig. 1a). This suggests that permanent sclerostin deficiency in these animals
14 overcomes the potential of these MSC to improve bone healing. In 2011, a study reported that
15 osteoblasts harvested whether from juvenile or adult mouse parietal bones demonstrated
16 reduced capacity for osteogenic differentiation when exposed to recombinant sclerostin,
17 already pointing out this protein as a promising target to abrogate in future tissue engineering
18 studies [80]. As expected, calvarial defects performed in *Sost* KO mice healed faster and better
19 than those performed in WT mice (Fig. 1a and Fig. 2b). These findings are consistent with other
20 studies conducted in the *Sost* KO mouse model or other mouse models targeting another
21 inhibitor of the Wnt/ β -catenin signaling pathway such as DKK1 (Dickkopf 1). In these studies,
22 higher bone formation was reported in the transgenic models compared with their WT
23 counterparts [11, 74, 81-83]. Regarding the high bone formation potential associated with
24 sclerostin deficiency, a complete healing of the bone defects left empty (no hydrogel) may have
25 been expected, in view of the reported finding that *Sost* KO mice were able to regenerate up
26 to 40% of the calvarial defect two months after surgery [81]. However, in this case, bone
27 formation was only observed at the edge of the defects and in a limited number of mice. In our
28 hands, defects left empty in *Sost* KO mice, as well as in WT mice treated with the Scl-Ab,
29 displayed very limited bone formation (Fig. 1a).
30
31
32
33
34
35
36
37
38
39
40
41
42
43
44
45
46
47
48
49
50
51
52
53
54
55
56
57
58
59
60
61
62
63
64
65

1 Quite remarkably, our data show that WT mice treated with mDPSC harvested from *Sost* KO
2 molar germs displayed a bone healing process significantly improved compared with WT mice
3 treated with WT cells (Fig. 1a-c). The bone quantity in these animals was comparable to their
4 *Sost* KO counterparts (Fig. 2 b). These important findings suggest that the local absence of
5 sclerostin in the MSC implanted in a bone defect has an equivalent benefit in terms of bone
6 regeneration to its complete deficiency. This is consistent with a previous study showing that
7 the local delivery of small active fragments of the sclerostin antibody loaded in Poly(lactide-
8 co-glycolide) microspheres and implanted within the fracture site favored bone healing in
9 ovariectomized (OVX) rats [84]. Noteworthy, Phase III clinical trials conducted in patients
10 with osteoporosis have shown that the systemic neutralization of sclerostin with a monoclonal
11 antibody was not devoid of adverse events, albeit very rare, such as osteoarthritis, arthralgia,
12 nasopharyngitis or back pain as well as an increased incidence of cardiovascular events [85,
13 86]. These studies have also unraveled a possible effect on the occurrence of osteonecrosis of
14 the jaw (ONJ). This later adverse event, albeit extremely rare (two cases reported in the
15 FRAME clinical trial) [87], is of particular importance in our prospect to develop a tissue
16 engineering strategy for the craniofacial skeleton. Quite reassuring, a recent study conducted
17 in OVX rats, in which experimental periodontitis was induced through ligature placement and
18 which were treated by either a sclerostin antibody or bisphosphonate, did not develop ONJ
19 under anti-sclerostin treatment while showing improved maxillary bone healing when
20 compared to animals treated with bisphosphonate [88]. However, the positive outcomes of our
21 present experiments conducted in WT mice treated with *Sost* KO mDPSC together with those
22 previously obtained with the local and controlled delivery of active fragments of a sclerostin
23 antibody [84], suggest that the local inhibition of sclerostin in a defect may be sufficient to
24 improve bone healing, while limiting the potential adverse events associated with a systemic
25 treatment.

1 Both clinical and preclinical studies have demonstrated that the major effect of the systemic
2 administration of a sclerostin antibody was the uncoupling of bone remodeling, leading to an
3 increase in bone formation [21, 89-92], and a decrease in bone resorption with lower
4 osteoclastic activity [93]. Here, we observed robust osteoblast activity evidenced by ALP
5 staining whenever sclerostin was deficient (Fig. 1b) or neutralized (Fig. 3b), coupled with no
6 impact on osteoclast activity in the defects (Fig. 2a and Fig. 4a). Furthermore, we found that
7 the porosity of the regenerated bone was improved by the antibody treatment compared to the
8 placebo but not by the addition of the MSC in the dense collagen hydrogels with sclerostin
9 deficiency (Fig. 2c) or neutralization (Fig. 4c). This micro-architecture parameter, which is
10 commonly used for the characterization of the cortical bone, is considered, when increased, as
11 a robust marker of bone fragility that might help to identify patients with increased risk of
12 fracture [94]. Therefore, together with our SHG observations showing improved organization
13 of the collagen fibers when sclerostin is inhibited or absent, we can conclude that sclerostin
14 deficiency or neutralization improved the quantity and the extracellular matrix organization of
15 the regenerated bone. However, this newly formed bone still needs to be further remodeled to
16 decrease its porosity and increase its density. Yet, our experiments were conducted in the
17 calvaria, which is a flat bone exposed to limited (although not negligible) mechanical
18 constraints [95]. These limited mechanical constraints may explain the lack of maturity
19 observed in the regenerated bone, even in *Sost* KO animals. Hence, we selected the calvarial
20 bone defect in first instance, as it is a critical and highly reproducible model [96]. In the future,
21 our tissue engineering approach combined with Scl-Ab should be explored in a more
22 mechanically solicited bone such as the mandible, either in rats or in larger animal models.
23
24
25
26
27
28
29
30
31
32
33
34
35
36
37
38
39
40
41
42
43
44
45
46
47
48
49
50
51
52
53
54
55

56 **5. Conclusions**

57
58
59
60
61
62
63
64
65

1 In conclusion, the sum of our work highlights that sclerostin neutralization by a monoclonal
2 antibody improved bone healing in a tissue engineering strategy for the craniofacial area.
3
4 Furthermore, similar outcome was observed with the implantation of MSC deficient for
5 sclerostin directly within the bone defect, suggesting that the local absence of this protein
6
7 during the bone healing process should be a therapeutic strategy to investigate, for instance via
8
9 the controlled delivery of the antibody from the tissue engineering construct. Beyond
10
11 sclerostin, monoclonal antibodies targeting other regulators of the bone remodeling process,
12
13 such as the RANK/RANKL pathway, are available and may be promising candidates to explore
14
15 further the potential of a combined therapeutic monoclonal antibody-tissue engineering
16
17 strategy for bone regeneration.
18
19
20
21
22
23
24
25

26 **Acknowledgements**

27
28 Experiments were supported by grants from Fondation des Gueules Cassées to URP2496.
29
30 Micro-CT device was funded by Fondation pour la Recherche Médicale for Plateforme
31
32 d'imagerie du Vivant Université de Paris and URP2496 (FRM DGE20111123012). SM PhD
33
34 was supported by Fondation des Gueules Cassées. Authors thank Jeremy Sadoine (URP2496
35
36 and PIV, Université de Paris, France) for his assistance and expertise regarding micro-CT
37
38 acquisitions and analyses, Sandy Ribes (URP 2496, Université de Paris, France) for her
39
40 assistance regarding mouse genotyping and immunohistochemistry analysis, Thomas Guilbert
41
42 (IMAG'IC, Institut Cochin, Paris, France) for his precious help in SHG, Dr Gael Rochefort
43
44 (SATT Lutech / Sorbonne University Alliance, Paris, France) for his scientific input.
45
46
47
48
49
50
51
52

53 **Data availability**

54
55 All the data are available upon request. Setrusumab (BPS804) was provided by Mereo
56
57 Biopharma (London, UK) through a Material transfer agreement (MTA).
58
59
60
61
62
63
64
65

References

- [1] Roberts SJ, Ke HZ. Anabolic Strategies to Augment Bone Fracture Healing. *Current osteoporosis reports* 2018;16:289-98.
- [2] Delgado-Calle J, Sato AY, Bellido T. Role and mechanism of action of sclerostin in bone. *Bone* 2017;96:29-37.
- [3] Poole KE, van Bezooijen RL, Loveridge N, Hamersma H, Papapoulos SE, Löwik CW, Reeve J. Sclerostin is a delayed secreted product of osteocytes that inhibits bone formation. *FASEB journal : official publication of the Federation of American Societies for Experimental Biology* 2005;19:1842-4.
- [4] Lin C, Jiang X, Dai Z, Guo X, Weng T, Wang J, Li Y, Feng G, Gao X, He L. Sclerostin mediates bone response to mechanical unloading through antagonizing Wnt/beta-catenin signaling. *Journal of bone and mineral research : the official journal of the American Society for Bone and Mineral Research* 2009;24:1651-61.
- [5] Li X, Zhang Y, Kang H, Liu W, Liu P, Zhang J, Harris SE, Wu D. Sclerostin binds to LRP5/6 and antagonizes canonical Wnt signaling. *The Journal of biological chemistry* 2005;280:19883-7.
- [6] Baron R, Kneissel M. WNT signaling in bone homeostasis and disease: from human mutations to treatments. *Nature medicine* 2013;19:179-92.
- [7] Compton JT, Lee FY. A review of osteocyte function and the emerging importance of sclerostin. *The Journal of bone and joint surgery American volume* 2014;96:1659-68.
- [8] Liu M, Kurimoto P, Zhang J, Niu QT, Stolina M, Dechow PC, Feng JQ, Hesterman J, Silva MD, Ominsky MS, Richards WG, Ke H, Kostenuik PJ. Sclerostin and DKK1 Inhibition Preserves and Augments Alveolar Bone Volume and Architecture in Rats with Alveolar Bone Loss. *Journal of dental research* 2018;97:1031-8.
- [9] Albiol L, Büttner A, Pflanz D, Mikolajewicz N, Birkhold AI, Kramer I, Kneissel M, Duda GN, Checa S, Willie BM. Effects of Long-Term Sclerostin Deficiency on Trabecular Bone Mass and Adaption to Limb Loading Differ in Male and Female Mice. *Calcified tissue international* 2020;106:415-30.
- [10] Collignon AM, Amri N, Lesieur J, Sadoine J, Ribes S, Menashi S, Simon S, Berdal A, Rochefort GY, Chaussain C, Gaucher C. Sclerostin Deficiency Promotes Reparative Dentinogenesis. *Journal of dental research* 2017;96:815-21.
- [11] Li C, Ominsky MS, Tan HL, Barrero M, Niu QT, Asuncion FJ, Lee E, Liu M, Simonet WS, Paszty C, Ke HZ. Increased callus mass and enhanced strength during fracture healing in mice lacking the sclerostin gene. *Bone* 2011;49:1178-85.
- [12] Fairfield H, Falank C, Harris E, Demambro V, McDonald M, Pettitt JA, Mohanty ST, Croucher P, Kramer I, Kneissel M, Rosen CJ, Reagan MR. The skeletal cell-derived molecule sclerostin drives bone marrow adipogenesis. *Journal of cellular physiology* 2018;233:1156-67.

- 1 [13] Stegen S, Stockmans I, Moermans K, Thienpont B, Maxwell PH, Carmeliet P,
2 Carmeliet G. Osteocytic oxygen sensing controls bone mass through epigenetic
3 regulation of sclerostin. *Nature communications* 2018;9:2557.
- 4 [14] Miyauchi A, Dinavahi RV, Crittenden DB, Yang W, Maddox JC, Hamaya E,
5 Nakamura Y, Libanati C, Grauer A, Shimauchi J. Increased bone mineral density for
6 1 year of romosozumab, vs placebo, followed by 2 years of denosumab in the
7 Japanese subgroup of the pivotal FRAME trial and extension. *Archives of*
8 *osteoporosis* 2019;14:59.
- 9 [15] Lewiecki EM, Dinavahi RV, Lazaretti-Castro M, Ebeling PR, Adachi JD,
10 Miyauchi A, Gielen E, Milmont CE, Libanati C, Grauer A. One Year of
11 Romosozumab Followed by Two Years of Denosumab Maintains Fracture Risk
12 Reductions: Results of the FRAME Extension Study. *Journal of bone and mineral*
13 *research : the official journal of the American Society for Bone and Mineral Research*
14 2019;34:419-28.
- 15 [16] McClung MR. Emerging Therapies for Osteoporosis. *Endocrinology and*
16 *metabolism (Seoul, Korea)* 2015;30:429-35.
- 17 [17] McClung MR, Grauer A, Boonen S, Bolognese MA, Brown JP, Diez-Perez A,
18 Langdahl BL, Reginster JY, Zanchetta JR, Wasserman SM, Katz L, Maddox J, Yang
19 YC, Libanati C, Bone HG. Romosozumab in postmenopausal women with low bone
20 mineral density. *The New England journal of medicine* 2014;370:412-20.
- 21 [18] Recknor CP, Recker RR, Benson CT, Robins DA, Chiang AY, Alam J, Hu L,
22 Matsumoto T, Sowa H, Sloan JH, Konrad RJ, Mitlak BH, Sipos AA. The Effect of
23 Discontinuing Treatment With Blososumab: Follow-up Results of a Phase 2
24 Randomized Clinical Trial in Postmenopausal Women With Low Bone Mineral
25 Density. *Journal of bone and mineral research : the official journal of the American*
26 *Society for Bone and Mineral Research* 2015;30:1717-25.
- 27 [19] Ralston SH, Gaston MS. Management of Osteogenesis Imperfecta. *Frontiers in*
28 *endocrinology* 2019;10:924.
- 29 [20] Glorieux FH, Devogelaer JP, Durigova M, Goemaere S, Hemsley S, Jakob F,
30 Junker U, Ruckle J, Seefried L, Winkle PJ. BPS804 Anti-Sclerostin Antibody in
31 Adults With Moderate Osteogenesis Imperfecta: Results of a Randomized Phase 2a
32 Trial. *Journal of bone and mineral research : the official journal of the American*
33 *Society for Bone and Mineral Research* 2017;32:1496-504.
- 34 [21] Fabre S, Funck-Brentano T, Cohen-Solal M. Anti-Sclerostin Antibodies in
35 Osteoporosis and Other Bone Diseases. *J Clin Med* 2020;9.
- 36 [22] Larsson S. Anti-sclerostin - is there an indication? *Injury* 2016;47 Suppl 1:S31-5.
- 37 [23] Cui L, Cheng H, Song C, Li C, Simonet WS, Ke HZ, Li G. Time-dependent
38 effects of sclerostin antibody on a mouse fracture healing model. *Journal of*
39 *musculoskeletal & neuronal interactions* 2013;13:178-84.
- 40 [24] Suen PK, He YX, Chow DH, Huang L, Li C, Ke HZ, Ominsky MS, Qin L.
41 Sclerostin monoclonal antibody enhanced bone fracture healing in an open
42 osteotomy model in rats. *Journal of orthopaedic research : official publication of the*
43 *Orthopaedic Research Society* 2014;32:997-1005.
- 44 [25] Virk MS, Alaei F, Tang H, Ominsky MS, Ke HZ, Lieberman JR. Systemic
45 administration of sclerostin antibody enhances bone repair in a critical-sized femoral
46 defect in a rat model. *The Journal of bone and joint surgery American volume*
47 2013;95:694-701.
- 48 [26] Alzahrani MM, Rauch F, Hamdy RC. Does Sclerostin Depletion Stimulate
49 Fracture Healing in a Mouse Model? *Clinical orthopaedics and related research*
50 2016;474:1294-302.

- 1 [27] Yee CS, Xie L, Hatsell S, Hum N, Muruges D, Economides AN, Loots GG,
2 Collette NM. Sclerostin antibody treatment improves fracture outcomes in a Type I
3 diabetic mouse model. *Bone* 2016;82:122-34.
- 4 [28] Yao Q, Ni J, Hou Y, Ding L, Zhang L, Jiang H. Expression of sclerostin scFv and
5 the effect of sclerostin scFv on healing of osteoporotic femur fracture in rats. *Cell*
6 *biochemistry and biophysics* 2014;69:229-35.
- 7 [29] Yao W, Dai W, Jiang L, Lay EY, Zhong Z, Ritchie RO, Li X, Ke H, Lane NE.
8 Sclerostin-antibody treatment of glucocorticoid-induced osteoporosis maintained
9 bone mass and strength. *Osteoporosis international : a journal established as result*
10 *of cooperation between the European Foundation for Osteoporosis and the National*
11 *Osteoporosis Foundation of the USA* 2016;27:283-94.
- 12 [30] Agholme F, Li X, Isaksson H, Ke HZ, Aspenberg P. Sclerostin antibody
13 treatment enhances metaphyseal bone healing in rats. *Journal of bone and mineral*
14 *research : the official journal of the American Society for Bone and Mineral Research*
15 *2010;25:2412-8.*
- 16 [31] Hu B, Li Y, Wang M, Zhu Y, Zhou Y, Sui B, Tan Y, Ning Y, Wang J, He J, Yang
17 C, Zou D. Functional reconstruction of critical-sized load-bearing bone defects using
18 a Sclerostin-targeting miR-210-3p-based construct to enhance osteogenic activity.
19 *Acta Biomater* 2018;76:275-82.
- 20 [32] Yorukoglu AC, Kiter AE, Akkaya S, Satiroglu-Tufan NL, Tufan AC. A Concise
21 Review on the Use of Mesenchymal Stem Cells in Cell Sheet-Based Tissue
22 Engineering with Special Emphasis on Bone Tissue Regeneration. *Stem cells*
23 *international* 2017;2017:2374161.
- 24 [33] La Noce M, Paino F, Spina A, Naddeo P, Montella R, Desiderio V, De Rosa A,
25 Papaccio G, Tirino V, Laino L. Dental pulp stem cells: state of the art and
26 suggestions for a true translation of research into therapy. *Journal of dentistry*
27 *2014;42:761-8.*
- 28 [34] Tatullo M, Marrelli M, Shakesheff KM, White LJ. Dental pulp stem cells: function,
29 isolation and applications in regenerative medicine. *Journal of tissue engineering*
30 *and regenerative medicine* 2015;9:1205-16.
- 31 [35] Kunimatsu R, Nakajima K, Awada T, Tsuka Y, Abe T, Ando K, Hiraki T, Kimura
32 A, Tanimoto K. Comparative characterization of stem cells from human exfoliated
33 deciduous teeth, dental pulp, and bone marrow-derived mesenchymal stem cells.
34 *Biochemical and biophysical research communications* 2018;501:193-8.
- 35 [36] Gronthos S, Mankani M, Brahimi J, Robey PG, Shi S. Postnatal human dental
36 pulp stem cells (DPSCs) in vitro and in vivo. *Proceedings of the National Academy of*
37 *Sciences of the United States of America* 2000;97:13625-30.
- 38 [37] Le Douarin NM, Calloni GW, Dupin E. The stem cells of the neural crest. *Cell*
39 *cycle (Georgetown, Tex)* 2008;7:1013-9.
- 40 [38] Quarto N, Wan DC, Kwan MD, Panetta NJ, Li S, Longaker MT. Origin matters:
41 differences in embryonic tissue origin and Wnt signaling determine the osteogenic
42 potential and healing capacity of frontal and parietal calvarial bones. *Journal of bone*
43 *and mineral research : the official journal of the American Society for Bone and*
44 *Mineral Research* 2010;25:1680-94.
- 45 [39] Chamieh F, Collignon AM, Coyac BR, Lesieur J, Ribes S, Sadoine J, Llorens A,
46 Nicoletti A, Letourneur D, Colombier ML, Nazhat SN, Bouchard P, Chaussain C,
47 Rochefort GY. Accelerated craniofacial bone regeneration through dense collagen
48 gel scaffolds seeded with dental pulp stem cells. *Scientific reports* 2016;6:38814.
- 49
50
51
52
53
54
55
56
57
58
59
60
61
62
63
64
65

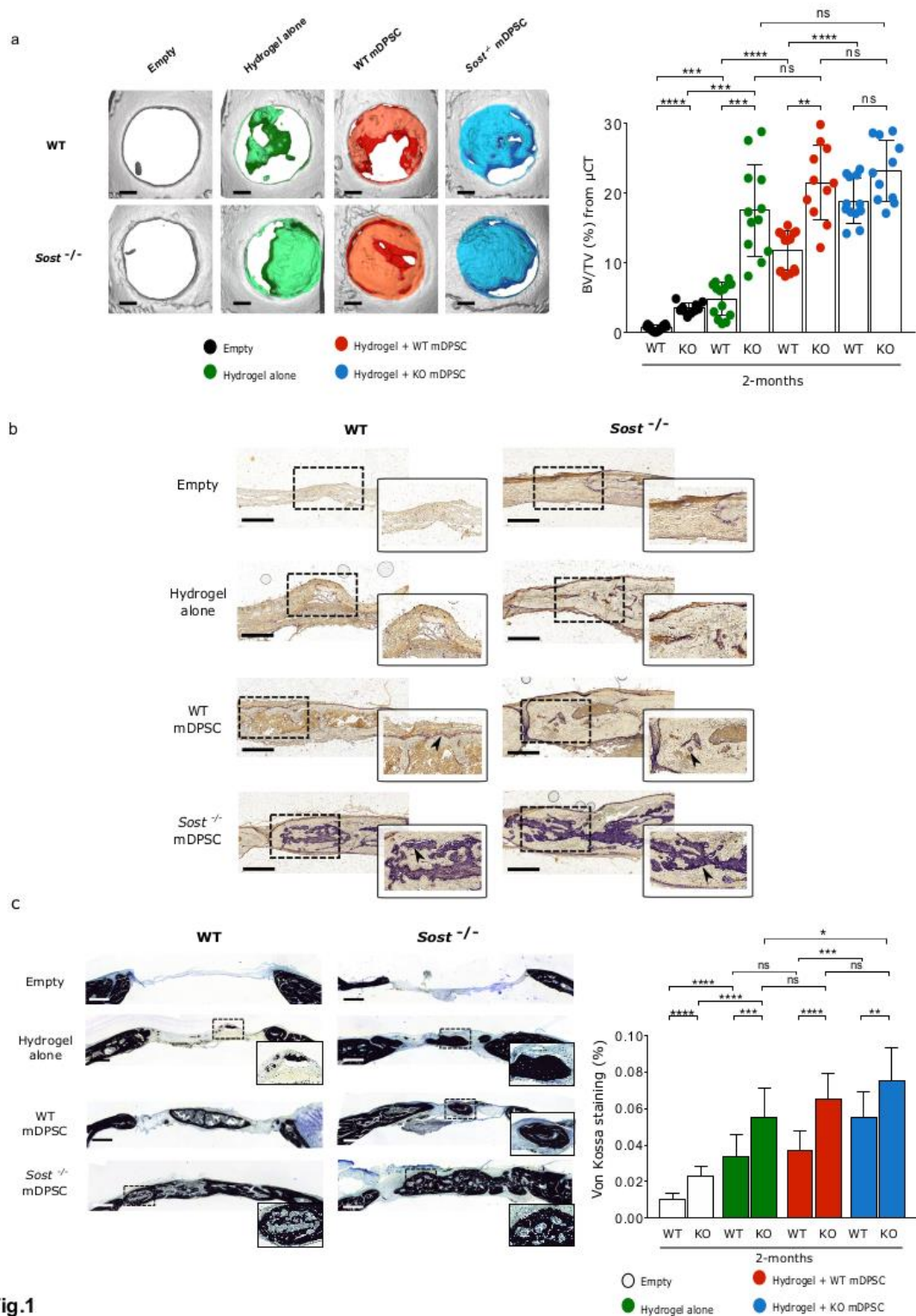
- 1 [40] Behnia A, Haghighat A, Talebi A, Nourbakhsh N, Heidari F. Transplantation of
2 stem cells from human exfoliated deciduous teeth for bone regeneration in the dog
3 mandibular defect. *World journal of stem cells* 2014;6:505-10.
- 4 [41] Leyendecker Junior A, Gomes Pinheiro CC, Lazzaretti Fernandes T, Franco
5 Bueno D. The use of human dental pulp stem cells for in vivo bone tissue
6 engineering: A systematic review. *Journal of tissue engineering*
7 2018;9:2041731417752766.
- 8 [42] Ramamoorthi M, Bakkar M, Jordan J, Tran SD. Osteogenic Potential of Dental
9 Mesenchymal Stem Cells in Preclinical Studies: A Systematic Review Using
10 Modified ARRIVE and CONSORT Guidelines. *Stem cells international*
11 2015;2015:378368.
- 12 [43] Novais A, Lesieur J, Sadoine J, Slimani L, Baroukh B, Saubaméa B, Schmitt A,
13 Vital S, Poliard A, Héлары C, Rochefort GY, Chaussain C, Gorin C. Priming Dental
14 Pulp Stem Cells from Human Exfoliated Deciduous Teeth with Fibroblast Growth
15 Factor-2 Enhances Mineralization Within Tissue-Engineered Constructs Implanted in
16 Craniofacial Bone Defects. *Stem cells translational medicine* 2019;8:844-57.
- 17 [44] Collignon AM, Castillo-Dali G, Gomez E, Guilbert T, Lesieur J, Nicoletti A,
18 Acuna-Mendoza S, Letourneur D, Chaussain C, Rochefort GY, Poliard A. Mouse
19 Wnt1-CRE-Rosa(Tomato) Dental Pulp Stem Cells Directly Contribute to the Calvarial
20 Bone Regeneration Process. *Stem cells (Dayton, Ohio)* 2019;37:701-11.
- 21 [45] Ho-Shui-Ling A, Bolander J, Rustom LE, Johnson AW, Luyten FP, Picart C.
22 Bone regeneration strategies: Engineered scaffolds, bioactive molecules and stem
23 cells current stage and future perspectives. *Biomaterials* 2018;180:143-62.
- 24 [46] Bose S, Li S, Mele E, Silberschmidt VV. Dry vs. wet: Properties and
25 performance of collagen films. Part II. Cyclic and time-dependent behaviours.
26 *Journal of the mechanical behavior of biomedical materials* 2020;112:104040.
- 27 [47] Qu HW, Fu HY, Han ZY, Sun Y. Biomaterials for bone tissue engineering
28 scaffolds: a review. *Rsc Adv* 2019;9:26252-62.
- 29 [48] Cen L, Liu W, Cui L, Zhang W, Cao Y. Collagen tissue engineering:
30 development of novel biomaterials and applications. *Pediatric research* 2008;63:492-
31 6.
- 32 [49] Ferreira AM, Gentile P, Chiono V, Ciardelli G. Collagen for bone tissue
33 regeneration. *Acta Biomater* 2012;8:3191-200.
- 34 [50] Koons GL, Diba M, Mikos AG. Materials design for bone-tissue engineering. *Nat*
35 *Rev Mater* 2020;5:584-603.
- 36 [51] Ajallouéian F, Nikogeorgos N, Ajallouéian A, Fossum M, Lee S, Chronakis IS.
37 Compressed collagen constructs with optimized mechanical properties and cell
38 interactions for tissue engineering applications. *International journal of biological*
39 *macromolecules* 2018;108:158-66.
- 40 [52] Coyac BR, Chicatun F, Hoac B, Nelea V, Chaussain C, Nazhat SN, McKee MD.
41 Mineralization of dense collagen hydrogel scaffolds by human pulp cells. *Journal of*
42 *dental research* 2013;92:648-54.
- 43 [53] Chicatun F, Pedraza CE, Ghezzi CE, Marelli B, Kaartinen MT, McKee MD,
44 Nazhat SN. Osteoid-mimicking dense collagen/chitosan hybrid gels.
45 *Biomacromolecules* 2011;12:2946-56.
- 46 [54] Guille MMG, Helary C, Vigier S, Nassif N. Dense fibrillar collagen matrices for
47 tissue repair. *Soft Matter* 2010;6:4963-7.
- 48 [55] Bitar M, Salih V, Brown RA, Nazhat SN. Effect of multiple unconfined
49 compression on cellular dense collagen scaffolds for bone tissue engineering.
50 *Journal of materials science Materials in medicine* 2007;18:237-44.
- 51
52
53
54
55
56
57
58
59
60
61
62
63
64
65

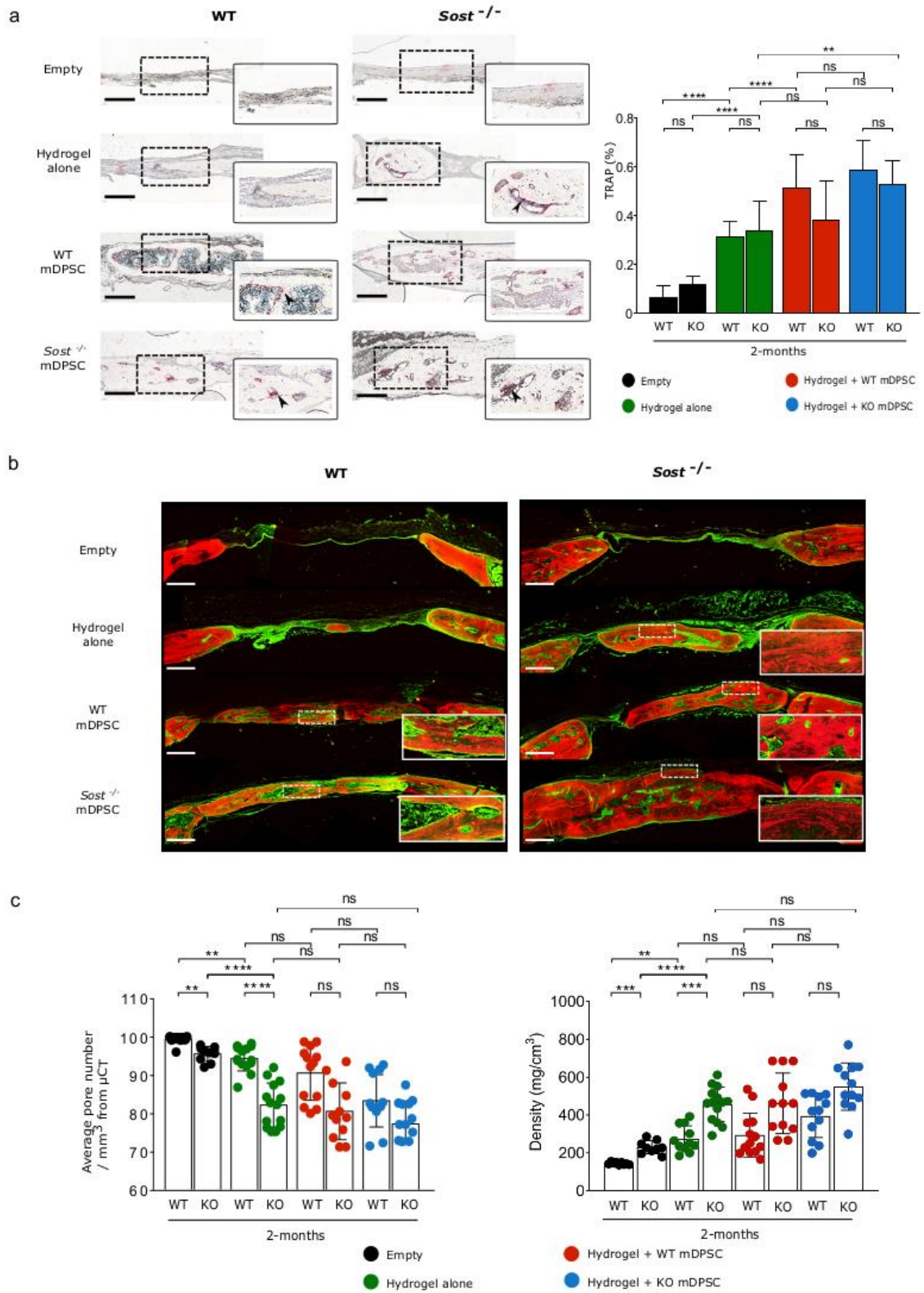
- 1 [56] Buxton PG, Bitar M, Gellynck K, Parkar M, Brown RA, Young AM, Knowles JC,
2 Nazhat SN. Dense collagen matrix accelerates osteogenic differentiation and
3 rescues the apoptotic response to MMP inhibition. *Bone* 2008;43:377-85.
- 4 [57] Gao C, Harvey EJ, Chua M, Chen BP, Jiang F, Liu Y, Li A, Wang H, Henderson
5 JE. MSC-seeded dense collagen scaffolds with a bolus dose of VEGF promote
6 healing of large bone defects. *European cells & materials* 2013;26:195-207;
7 discussion
- 8 [58] Griffanti G, Nazhat SN. Dense fibrillar collagen-based hydrogels as functional
9 osteoid-mimicking scaffolds. *Int Mater Rev* 2020;65:502-21.
- 10 [59] Leach DG, Young S, Hartgerink JD. Advances in immunotherapy delivery from
11 implantable and injectable biomaterials. *Acta Biomater* 2019;88:15-31.
- 12 [60] Wang C, Ye Y, Hu Q, Bellotti A, Gu Z. Tailoring Biomaterials for Cancer
13 Immunotherapy: Emerging Trends and Future Outlook. *Advanced materials* 2017;29.
- 14 [61] Weber JS, Mule JJ. Cancer immunotherapy meets biomaterials. *Nature*
15 *biotechnology* 2015;33:44-5.
- 16 [62] Roschger A, Roschger P, Keplinger P, Klaushofer K, Abdullah S, Kneissel M,
17 Rauch F. Effect of sclerostin antibody treatment in a mouse model of severe
18 osteogenesis imperfecta. *Bone* 2014;66:182-8.
- 19 [63] Abou Neel EA, Bozec L, Knowles JC, Syed O, Mudera V, Day R, Hyun JK.
20 Collagen--emerging collagen based therapies hit the patient. *Advanced drug delivery*
21 *reviews* 2013;65:429-56.
- 22 [64] Brown RA, Wiseman M, Chuo CB, Cheema U, Nazhat SN. Ultrarapid
23 engineering of biomimetic materials and tissues: Fabrication of nano- and
24 microstructures by plastic compression. *Adv Funct Mater* 2005;15:1762-70.
- 25 [65] Rajan N, Habermehl J, Cote MF, Doillon CJ, Mantovani D. Preparation of ready-
26 to-use, storable and reconstituted type I collagen from rat tail tendon for tissue
27 engineering applications. *Nature protocols* 2006;1:2753-8.
- 28 [66] Pedraza CE, Marelli B, Chicatun F, McKee MD, Nazhat SN. An in vitro
29 assessment of a cell-containing collagenous extracellular matrix-like scaffold for
30 bone tissue engineering. *Tissue engineering Part A* 2010;16:781-93.
- 31 [67] Spicer PP, Kretlow JD, Young S, Jansen JA, Kasper FK, Mikos AG. Evaluation
32 of bone regeneration using the rat critical size calvarial defect. *Nature protocols*
33 2012;7:1918-29.
- 34 [68] Rosset A, Spadola L, Ratib O. OsiriX: an open-source software for navigating in
35 multidimensional DICOM images. *Journal of digital imaging* 2004;17:205-16.
- 36 [69] Bouxsein ML, Boyd SK, Christiansen BA, Guldborg RE, Jepsen KJ, Muller R.
37 Guidelines for assessment of bone microstructure in rodents using micro-computed
38 tomography. *Journal of bone and mineral research : the official journal of the*
39 *American Society for Bone and Mineral Research* 2010;25:1468-86.
- 40 [70] Lafont J, Baroukh B, Berdal A, Colombier ML, Barritault D, Caruelle JP, Saffar
41 JL. RGTA11, a new healing agent, triggers developmental events during healing of
42 craniotomy defects in adult rats. *Growth factors* 1998;16:23-38.
- 43 [71] Schindelin J, Arganda-Carreras I, Frise E, Kaynig V, Longair M, Pietzsch T,
44 Preibisch S, Rueden C, Saalfeld S, Schmid B, Tinevez JY, White DJ, Hartenstein V,
45 Eliceiri K, Tomancak P, Cardona A. Fiji: an open-source platform for biological-image
46 analysis. *Nature methods* 2012;9:676-82.
- 47 [72] Guilbert T, Odin C, Le Grand Y, Gailhouste L, Turlin B, Ezan F, Desille Y, Baffet
48 G, Guyader D. A robust collagen scoring method for human liver fibrosis by second
49 harmonic microscopy. *Optics express* 2010;18:25794-807.
- 50
51
52
53
54
55
56
57
58
59
60
61
62
63
64
65

- 1 [73] Collignon AM, Lesieur J, Anizan N, Azzouna RB, Poliard A, Gorin C, Letourneur
2 D, Chaussain C, Rouzet F, Rochefort GY. Early angiogenesis detected by PET
3 imaging with (64)Cu-NODAGA-RGD is predictive of bone critical defect repair. *Acta*
4 *Biomater* 2018;82:111-21.
- 5 [74] McGee-Lawrence ME, Ryan ZC, Carpio LR, Kakar S, Westendorf JJ, Kumar R.
6 Sclerostin deficient mice rapidly heal bone defects by activating β -catenin and
7 increasing intramembranous ossification. *Biochemical and biophysical research*
8 *communications* 2013;441:886-90.
- 9 [75] Pathak JL, Bravenboer N, Klein-Nulend J. The Osteocyte as the New Discovery
10 of Therapeutic Options in Rare Bone Diseases. *Frontiers in endocrinology*
11 2020;11:405.
- 12 [76] Russow G, Jahn D, Appelt J, Mardian S, Tsitsilonis S, Keller J. Anabolic
13 Therapies in Osteoporosis and Bone Regeneration. *International journal of molecular*
14 *sciences* 2018;20.
- 15 [77] Santagati F, Rijli FM. Cranial neural crest and the building of the vertebrate
16 head. *Nat Rev Neurosci* 2003;4:806-18.
- 17 [78] Senarath-Yapa K, Li S, Meyer NP, Longaker MT, Quarto N. Integration of
18 multiple signaling pathways determines differences in the osteogenic potential and
19 tissue regeneration of neural crest-derived and mesoderm-derived calvarial bones.
20 *International journal of molecular sciences* 2013;14:5978-97.
- 21 [79] Bitar M, Brown RA, Salih V, Kidane AG, Knowles JC, Nazhat SN. Effect of cell
22 density on osteoblastic differentiation and matrix degradation of biomimetic dense
23 collagen scaffolds. *Biomacromolecules* 2008;9:129-35.
- 24 [80] Kwan MD, Quarto N, Gupta DM, Slater BJ, Wan DC, Longaker MT. Differential
25 expression of sclerostin in adult and juvenile mouse calvariae. *Plastic and*
26 *reconstructive surgery* 2011;127:595-602.
- 27 [81] Kang KS, Lastfogel J, Ackerman LL, Jea A, Robling AG, Tholpady SS. Loss of
28 mechanosensitive sclerostin may accelerate cranial bone growth and regeneration.
29 *Journal of neurosurgery* 2018;129:1085-91.
- 30 [82] Colditz J, Thiele S, Baschant U, Niehrs C, Bonewald LF, Hofbauer LC, Rauner
31 M. Postnatal Skeletal Deletion of Dickkopf-1 Increases Bone Formation and Bone
32 Volume in Male and Female Mice, Despite Increased Sclerostin Expression. *Journal*
33 *of bone and mineral research : the official journal of the American Society for Bone*
34 *and Mineral Research* 2018;33:1698-707.
- 35 [83] Schupbach D, Comeau-Gauthier M, Harvey E, Merle G. Wnt modulation in bone
36 healing. *Bone* 2020;138:115491.
- 37 [84] Li M, Li S, Liu J, Cui X, Zhang S, Zhou J, Wang X, Yao Q. Sustained-release of
38 sclerostin single-chain antibody fragments using poly(lactic-co-glycolic acid)
39 microspheres for osteoporotic fracture repair. *Journal of biomedical materials*
40 *research Part A* 2019;107:1832-40.
- 41 [85] Iolascon G, Moretti A, Toro G, Gimigliano F, Liguori S, Paoletta M.
42 *Pharmacological Therapy of Osteoporosis: What's New? Clinical interventions in*
43 *aging* 2020;15:485-91.
- 44 [86] Canalis E. MANAGEMENT OF ENDOCRINE DISEASE: Novel anabolic
45 treatments for osteoporosis. *European journal of endocrinology* 2018;178:R33-R44.
- 46 [87] Saag KG, Petersen J, Brandi ML, Karaplis AC, Lorentzon M, Thomas T, Maddox
47 J, Fan M, Meisner PD, Grauer A. Romosozumab or Alendronate for Fracture
48 Prevention in Women with Osteoporosis. *The New England journal of medicine*
49 2017;377:1417-27.
- 50
51
52
53
54
55
56
57
58
59
60
61
62
63
64
65

1 [88] Hadaya D, Gkouveris I, Soundia A, Bezouglaia O, Boyce RW, Stolina M, Dwyer
2 D, Dry SM, Pirihi FQ, Aghaloo TL, Tetradis S. Clinically Relevant Doses of Sclerostin
3 Antibody Do Not Induce Osteonecrosis of the Jaw (ONJ) in Rats with Experimental
4 Periodontitis. *Journal of bone and mineral research : the official journal of the*
5 *American Society for Bone and Mineral Research* 2019;34:171-81.
6 [89] Ominsky MS, Niu QT, Li C, Li X, Ke HZ. Tissue-level mechanisms responsible
7 for the increase in bone formation and bone volume by sclerostin antibody. *Journal*
8 *of bone and mineral research : the official journal of the American Society for Bone*
9 *and Mineral Research* 2014;29:1424-30.
10 [90] Appelman-Dijkstra NM, Papapoulos SE. Sclerostin Inhibition in the Management
11 of Osteoporosis. *Calcified tissue international* 2016;98:370-80.
12 [91] Ren Y, Han X, Ho SP, Harris SE, Cao Z, Economides AN, Qin C, Ke H, Liu M,
13 Feng JQ. Removal of SOST or blocking its product sclerostin rescues defects in the
14 periodontitis mouse model. *FASEB journal : official publication of the Federation of*
15 *American Societies for Experimental Biology* 2015;29:2702-11.
16 [92] Balani DH, Trinh S, Xu M, Kronenberg HM. Sclerostin Antibody Administration
17 Increases the Numbers of Sox9creER+ Skeletal Precursors and Their Progeny.
18 *Journal of bone and mineral research : the official journal of the American Society for*
19 *Bone and Mineral Research* 2021;36:757-67.
20 [93] Glass DA, 2nd, Bialek P, Ahn JD, Starbuck M, Patel MS, Clevers H, Taketo MM,
21 Long F, McMahon AP, Lang RA, Karsenty G. Canonical Wnt signaling in
22 differentiated osteoblasts controls osteoclast differentiation. *Dev Cell* 2005;8:751-64.
23 [94] Farr JN, Khosla S. Skeletal changes through the lifespan--from growth to
24 senescence. *Nature reviews Endocrinology* 2015;11:513-21.
25 [95] Falland-Cheung L, Waddell JN, Chun Li K, Tong D, Brunton P. Investigation of
26 the elastic modulus, tensile and flexural strength of five skull simulant materials for
27 impact testing of a forensic skin/skull/brain model. *Journal of the mechanical*
28 *behavior of biomedical materials* 2017;68:303-7.
29 [96] Wang D, Gilbert JR, Zhang X, Zhao B, Ker DFE, Cooper GM. Calvarial Versus
30 Long Bone: Implications for Tailoring Skeletal Tissue Engineering. *Tissue*
31 *engineering Part B, Reviews* 2020;26:46-63.
32
33
34
35
36
37
38
39
40
41
42
43
44
45
46
47
48
49
50
51
52
53
54
55
56
57
58
59
60
61
62
63
64
65

1
2
3
4
5
6
7
8
9
10
11
12
13
14
15
16
17
18
19
20
21
22
23
24
25
26
27
28
29
30
31
32
33
34
35
36
37
38
39
40
41
42
43
44
45
46
47
48
49
50
51
52
53
54
55
56
57
58
59
60
61
62
63
64
65





1
2
3
4
5
6
7
8
9
10
11
12
13
14
15
16
17
18
19
20
21
22
23
24
25
26
27
28
29
30
31
32
33
34
35
36
37
38
39
40
41
42
43
44
45
46
47
48
49
50
51
52
53
54
55
56
57
58
59
60
61
62
63
64
65

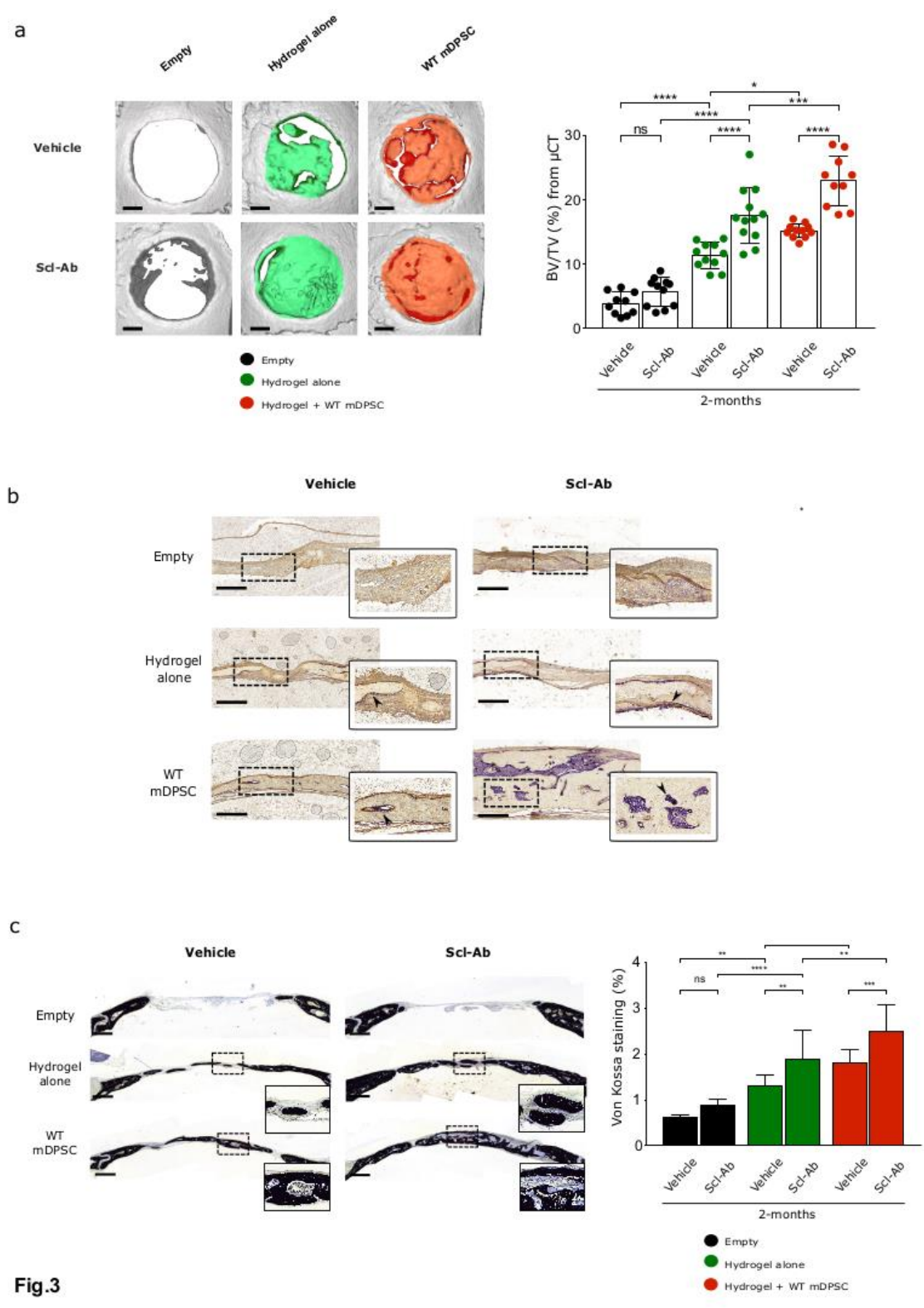


Fig.3

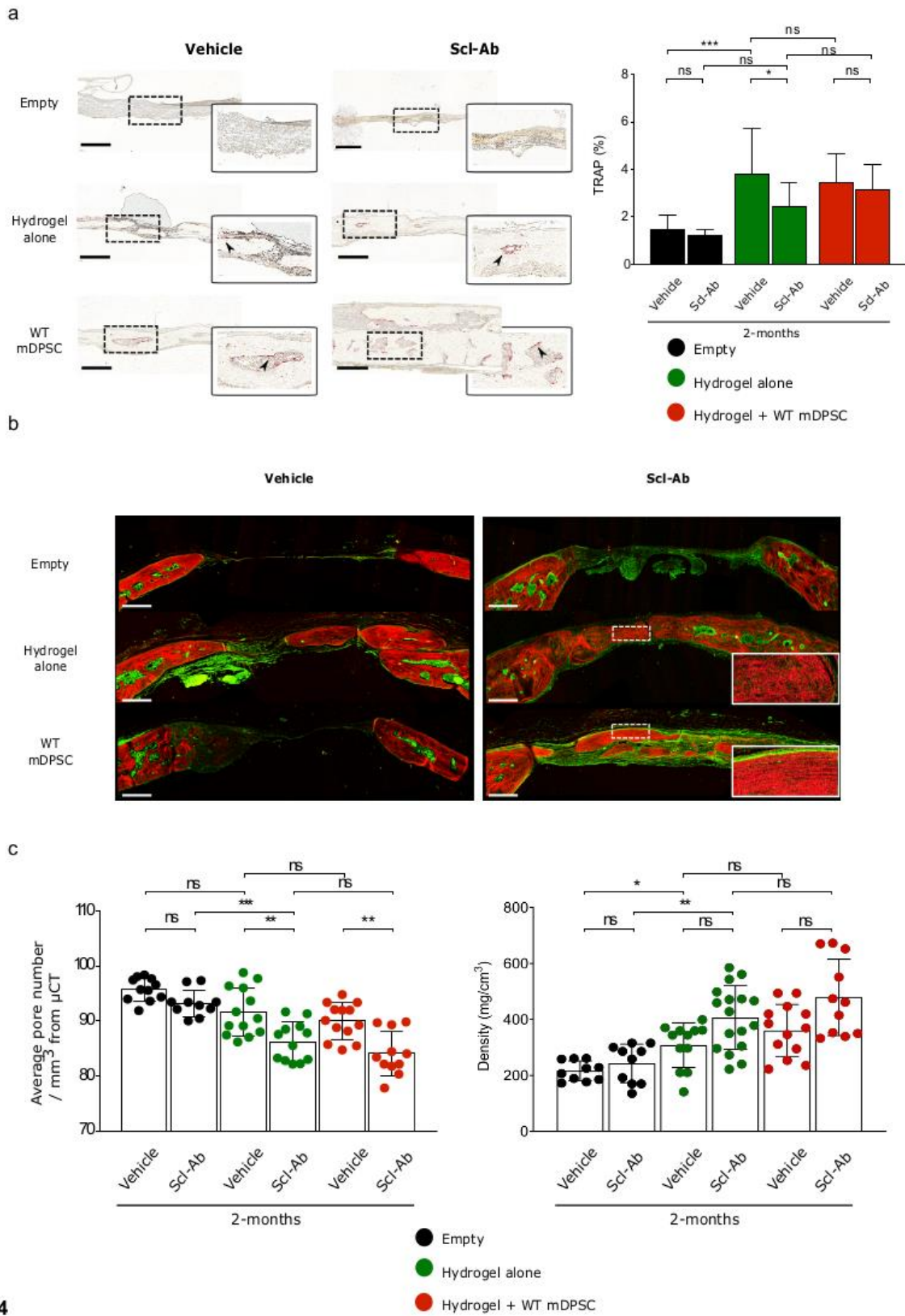


Figure captions

Figure 1: Bone formation within the defect at two months.

- a) Representative three dimensional images of bone defects created in WT and *Sost* KO mice in four conditions: defect left empty, defect filled with acellular hydrogel, hydrogel seeded WT mDPSC and hydrogel seeded *Sost* KO mDPSC. Black color represents the empty defect, green color represents newly formed bone in a defect filled with acellular hydrogel, red color represents newly formed bone in a defect filled with a hydrogel seeded with WT mDPSC and blue color represents newly formed bone in a defect filled with a hydrogel seeded with *Sost* KO mDPSC. Newly formed bone volumetric fraction is expressed as a percentage of volume (BV/TV) on the total area of the defect from micro-CT analysis. Data showed that *Sost* KO mice presented a significantly higher BV/TV compared to their WT counterparts and that WT mice treated with *Sost* KO mDPSC-seeded hydrogels displayed a similar BV/TV compared to *Sost* KO mice.
- b) Staining of osteoblastic-associated alkaline phosphatase (ALP) activity was investigated to assess bone formation by osteoblasts. ALP activity, in purple, was strong in WT mice treated with *Sost* KO cells and in *Sost* KO mice, especially those treated with *Sost* KO cells. Inset detail shows the area of interest with ALP signals indicated by arrows at higher magnification (x 40).
- c) Mineral formation in calvarial bone defects revealed by Von Kossa staining. Inset detail displays the area of interest at higher magnification (x 40). Quantitative analysis of Von Kossa staining in % have been performed in four conditions: defect left empty, defect filled with acellular hydrogel, hydrogel seeded WT mDPSC and hydrogel seeded *Sost* KO mDPSC. Black color represents the empty defect, green color represents newly formed bone in a defect filled with acellular hydrogel, red color

represents newly formed bone in a defect filled with a hydrogel seeded with WT mDPSC and blue color represents newly formed bone in a defect filled with a hydrogel seeded with *Sost* KO mDPSC. Results showed that mineral formation was significantly higher in WT and *Sost* KO mice treated with *Sost* KO mDPSC.

Scale bars: a) 1 mm, b) 250 μm c) 400 μm . Values represent mean \pm SD: ns: not significant; * $P < 0.05$; ** $P < 0.01$, *** $P < 0.001$ and **** $P < 0.0001$ with a Brown-Forsythe and Welch ANOVA test.

Figure 2: Characterization of newly formed bone in WT and *Sost* KO mice at two months.

- a) Staining of osteoclastic tartrate-resistant acid phosphatase (TRAP) activity images on WT and *Sost* KO mice in defects filled with WT and *Sost* KO mDPSC. Inset detail displays, at higher magnification (x 40), TRAP signals in rose red indicated by arrows. Quantification of TRAP activity (%) has been performed: black color represents the empty defect, green color represents newly formed bone in a defect filled with acellular hydrogel, red color represents newly formed bone in a defect filled with a hydrogel seeded with WT mDPSC and blue color represents newly formed bone in a defect filled with a hydrogel seeded with *Sost* KO mDPSC. Results showed no significant difference between the cellularized scaffold groups at this stage of the repair process.
- b) Images from second harmonic generation (SHG) microscopy showed large amount of red-labeled well-organized bundles of collagen fibers within the defects performed in *Sost* KO mice for all the conditions (acellular hydrogel, hydrogel seeded with WT mDPSC and *Sost* KO mDPSC) and in WT mice treated with *Sost* KO cells. Inset detail shows the area of interest at higher magnification (x 40).
- c) Quantitative analysis of bone porosity (mm^{-3}) and density (mg/cm^3) from micro-CT acquisitions showing no improvement of these microarchitecture parameters in the

cellularized scaffold groups at this stage of the repair process. Black color represents the empty defect, green color represents newly formed bone in a defect filled with acellular hydrogel, red color represents newly formed bone in a defect filled with a hydrogel seeded with WT mDPSC and blue color represents newly formed bone in a defect filled with a hydrogel seeded with *Sost* KO mDPSC.

Scale bar: **a)** 250 μm , **b)** 500 μm . Values represent mean \pm SD: ns: not significant; * $P < 0.05$; ** $P < 0.01$, *** $P < 0.001$ and **** $P < 0.0001$ with a Brown-Forsythe and Welch ANOVA test.

Figure 3: Bone formation within calvarial defect in WT mice after Sclerostin antibody injection at two months.

- a) Representative three dimensional images of bone defects created in WT mice either after Scl-AB or vehicle injection, in three conditions: defect left empty, defect filled with acellular hydrogel, defect filled with hydrogel seeded WT mDPSC. Black color represents the empty defect, green color represents newly formed bone in a defect filled with acellular hydrogel and red color represents newly formed bone in a defect filled with a hydrogel seeded with WT mDPSC. Newly formed bone volumetric fraction expressed as a percentage of volume (BV/TV) on the total area of the defect from micro-CT analysis is represented. Micro-CT analysis showed significantly higher BV/TV in animals that received Scl-Ab injection when compared to vehicle in the condition “acellular hydrogel” and “hydrogel seeded with WT mDPSC”. In the Scl-Ab treated mice, the addition of cells in the hydrogels significantly enhanced bone formation.
- b) Staining of osteoblastic-associated alkaline phosphatase (ALP) activity was investigated to determine whether the Scl-Ab treatment impacted bone formation by osteoblasts. ALP activity, in purple, was strong in mice that received Scl-Ab treatment

and cellularized hydrogels. Inset detail shows the area of interest with ALP signals indicated by arrows at higher magnification (x 40).

- c) Mineral formation in calvarial bone defects revealed by Von Kossa staining. Inset detail displays the area of interest at higher magnification (x 40). Quantitative analysis of Von Kossa staining in % was performed for the three conditions: defect left empty, defect filled with acellular hydrogel and hydrogel seeded WT mDPSC. Black color represents the empty defect, green color represents newly formed bone in a defect filled with acellular hydrogel and red color represents newly formed bone in a defect filled with a hydrogel seeded with WT mDPSC. Results showed that mineral formation was significantly increased in the conditions “acellular hydrogel” and “hydrogel seeded with WT mDPSC” in mice that received Scl-AB injection compare to vehicle group. Furthermore, in the Scl-Ab treated mice, the addition of cells in the hydrogels significantly enhanced bone formation.

Scale bars: **a)** 1 mm **b)** 250 μ m **c)** 400 μ m. Values represent mean \pm SD: ns: not significant;

* $P < 0.05$; ** $P < 0.01$, *** $P < 0.001$ and **** $P < 0.0001$ with a Brown-Forsythe and Welch ANOVA test.

Figure 4: Characterization of newly formed bone after Sclerostin antibody injection at two months

- a) Staining of osteoclastic tartrate-resistant acid phosphatase (TRAP) activity images in mice treated with Scl-Ab or vehicle. Inset detail shows TRAP signals in rose red indicated by arrows at higher magnification (x 40). Quantification of TRAP activity (%) was performed for the three conditions: black color represents the empty defect, green color the newly formed bone in a defect filled with acellular hydrogel, and red color the newly formed bone in a defect filled with a hydrogel seeded with WT mDPSC. Results showed significant lower activity for the condition “acellular

hydrogel” in mice that received Scl-Ab and no difference was found in the cellularized groups.

- b) Representative images from second harmonic generation (SHG) microscopy revealed red-stained better-organized collagen fibers in mice treated with the Scl-AB when compared to the vehicle for the conditions “acellular hydrogel” and “hydrogel seeded with WT mDPSC”. Inset detail shows the area of interest at higher magnification (x 40).
- c) Quantitative analysis of bone porosity (mm^{-3}) and density (mg/cm^3) from Micro-CT have been performed in three conditions: black color represents the empty defect, green color the newly formed bone in a defect filled with acellular hydrogel, and red color the newly formed bone in a defect filled with a hydrogel seeded with WT mDPSC. Porosity analysis revealed significantly lower porosity in defects performed in animals treated with the Scl-Ab for the conditions “acellular hydrogel” and “hydrogel seeded with WT mDPSC”.

Scale bar: **a)** 250 μm , **b)** 500 μm . Values represent mean \pm SD: ns: not significant; * $P < 0.05$; ** $P < 0.01$, *** $P < 0.001$ and **** $P < 0.0001$ with a Brown-Forsythe and Welch ANOVA test.